CO Hydrogenation Reaction on Sulfided Molybdenum Catalysts

Xue-Rong Shi[1,2], Haijun Jiao[1,3], Klaus Hermann[2*], and Jianguo Wang[1*]

1) *State Key Laboratory of Coal Conversion, Institute of Coal Chemistry, Chinese Academy of Sciences, Taiyuan, Shanxi 030001 (China).*
2) *Theory Department, Fritz-Haber-Institut der MPG, Faradayweg 4-6, D-14195 Berlin and Collaborative Research Center Sfb 546, Berlin (Germany).*
3) *Leibniz-Institut für Katalyse e.V. an der Universität Rostock, Albert-Einstein-Strasse 29a, 18059 Rostock (Germany).*

* Corresponding authors: K. Hermann (hermann@fhi-berlin.mpg.de);
J. Wang (iccjgw@sxicc.ac.cn)

Keywords: CO hydrogenation, molybdenum disulfide, intermediate surface species, DFT studies.

ABSTRACT

Adsorption of reaction intermediates appearing during CO hydrogenation at the sulfur covered MoS_2(10-10) surfaces, Mo-termination with 42% S coverage and S-termination with 50% S coverage, are investigated systematically using periodic density functional theory methods. Computed vibrational frequencies of all intermediates are compared with observed data from infrared (IR) spectroscopy allowing a detailed interpretation and assignment of the different features in the experimental spectra. The pathway for CO hydrogenation on both terminations has been studied in detail where the most likely reaction path involves C_1 type surface species in the sequence

$$CO \rightarrow CHO \rightarrow CH_2O \rightarrow CH_2OH \rightarrow CH_2 \rightarrow CH_3 \rightarrow CH_4$$

in agreement with experiment.

1. INTRODUCTION

Sulfided Mo catalysts have been widely used in hydrodesulfurization (HDS) and hydrodenitrogenation (HDN) processes and exhibit also high activity for methanation and for the Fischer-Tropsch synthesis of light hydrocarbons from CO hydrogenation [1−7]. In particular, CO hydrogenation on sulfided Mo catalysts has been studied extensively because of the tolerance of these catalysts to sulfur poisoning [2−7]. Using *in-situ* diffuse reflectance infrared Fourier transform (DRIFT) spectroscopy, Koizumi et al. [8] identified the main products of CO hydrogenation on pure MoS_2 catalyst to be CO_2 and CH_4. However, the modification of the pure MoS_2 surface by alkali promoters yields alcohols instead of hydrocarbons as while additional promoters, such as Ni or Co, are found to increase the selectivity of ethanol and higher alcohols [9−11].

The CO hydrogenation mechanism, involving formation and breaking of C-H, O-H, and C-C bonds, is rather complicated and various reaction schemes have been proposed [12−15] so far. The basic process has been described by reaction steps (1)

$$CO + 3H \rightarrow CHO + 2H \rightarrow CH_2O + H \rightarrow CH_3O \qquad (1)$$

occurring at the catalyst surface followed by competing steps (2) [16]

- $CH_3O + 2H \rightarrow CH_3 + (H_2O)_{gas}$ followed by
  $CH_3 + H \rightarrow (CH_4)_{gas}$ or by $CH_3 + CO + 3H \rightarrow (CH_3CH_2OH)_{gas}$ (2a)
- $CH_3O + H \rightarrow (CH_3OH)_{gas}$ (2b)
- $CH_3O + CO + H \rightarrow CH_3COO + H \rightarrow (HCOOCH_3)_{gas}$ (2c)

producing alcohols (steps (2a), (2b)) or formate (steps (2c), the latter will also form alcohols in subsequent reaction steps). In this context, the existence and details of reaction intermediates have been discussed for a long time but still remain unclear. As examples we mention temperature programmed desorption (TPD) experiments that suggest that formyl (CHO) intermediates are formed at the catalyst surface which, depending on the reaction conditions and the nature of the active sites, may be hydrogenated to yield alcohols or may react to form other hydrocarbons [17−19]. It is also suggested that the primary product is methanol and the methanol could then undergo secondary reactions to produce methane. H_2O and CO_2 formation may take place before methanol desorbing from the surface during high-pressure CO hydrogenation. Further, experiments of CO hydrogena-

tion on a sulfided Mo/γ-Al_2O_3 catalyst using *in-situ* DRIFT spectroscopy show vibrational frequency bands where those at 1590, 1420 and 1385 cm^{-1} are claimed to indicate surface formate (HCOO), while an additional band at 1470 cm^{-1} could originate from acetate (CH_3COO), methoxy (CH_3O), or from carbonate (CO_3) species [8]. Despite these experimental efforts theoretical work has been restricted mainly to CO, H_2 adsorption and surface properties of MoS_2 [20−31]. Using a periodic two-sheet model (for the definition of sheets see Sec. 2 below) of the ideal MoS_2(10-10) surface, Cristol et al. [29] found that dissociative H_2 adsorption is endothermic at the Mo terminated sheet with 50% S coverage while it is exothermic for 33% S coverage forming one S-H and one Mo-H group.

Using a periodic single-sheet model, Sun et al. [28] studied H_2 adsorption and dissociation on MoS_2 and NiMoS, and found that homolytic H_2 dissociation to form two S-H groups is thermodynamically preferred over heterolytic dissociation yielding one S-H and one Mo-H group, and the latter is kinetically favored. On the other hand, Bollinger et al. [27] found the most stable hydrogen adsorption to be the formation of two S-H groups on the S edge. By means of IR spectroscopy and applying a two-sheet periodic model Travert et al. [32] reported CO adsorption on sulfided Mo catalysts and compared the results of spectroscopic with theoretical studies. They found that under reductive condition adsorption of one CO molecule at the sulfur edge with about 50% S coverage is the most stable and exothermic by 0.7 eV. They also identified three thermodynamically stable surfaces for different H_2/H_2S pressure ratios which were also studied by Schweiger et al. [24], Bollinger et al. [27], Raybaud et al. [33] and Cristol et al. [34].

While a considerable amount of experimental studies have been carried out, theoretical investigations on CO hydrogenation at the pure MoS_2 surface are still lacking. Recently, Huang and Cho have studied CO hydrogenation at the MoS_2(10-10) surface [35] where they considering two terminations reflecting full Mo metal and full sulfur coverage. They found that the most likely products of CO hydrogenation are CH_4 and CO_2, in agreement with the experiment results [8]. However, according to the studies of Travert et al. [32], Cristol et al. [29,34], Raybaud et al. [33], and Sun et al. [28,36], the two terminations considered by Huang and Cho [35] do not seem to reflect the realistic catalyst. They are not stable for H_2S/H_2 pressure ratios in the range $0.0001 < p(H_2S)/p(H_2) < 10000$ [34]. For $p(H_2S)/p(H_2) < 0.05$ corresponding to the realistic catalytic system the MoS_2(10-10) surface is terminated by Mo metal sheets covered with about 50% sulfur and by S sheets with about

50% sulfur vacancies [28,29,32−34,36] as mentioned above. These terminations have been considered in the present work.

We apply ab initio density functional theory (DFT) methods together with periodic surface models to examine all intermediates of the above described CO hydrogenation reaction steps [16]. We focus on geometric and energetic parameters of the adsorbed species as well as on their vibrational properties in connection with the interpretation of the corresponding experimental data from IR measurements. The intermediates are C_1-type CH_x, CH_xOH (x = 0, 1, 2), CH_xO (x = 1, 2, 3), HCOO and CO_3 which lead to C_1-type products found over pure MoS_2 catalysts [16]. We also consider C_2-type intermediates CH_3COO, CH_3CO, CH_3CHO and CH_3CH_2O. In addition, possible reaction paths of CO hydrogenation have been explored.

Sec. 2 describes briefly model geometries and computational methods while Sec. 3 presents the theoretical results and discussion. Finally, we summarize our conclusions in Sec. 4.

2. THEORETICAL DETAILS

Clean MoS_2 forms a hexagonal lattice with two elemental units in the elementary cell. The lattice is layer type with weakly coupling MoS_2 sheets oriented along the (0001) direction of the crystal. The orientation of the reactive surface is assumed to be (10-10) [36] where the ideal bulk terminated geometry is described by parallel pairs of MoS_2 sheets perpendicular to the surface (Fig. 1a). Each pair consists of two differently terminated sheets, one of Mo and one of S termination which may offer active sites for catalytic reactions. Theoretical thermodynamic studies on the MoS_2(10-10) surface at different H_2S/H_2 exposures [28,29,32−34,36] have shown that under hydrogen-rich conditions i.e.; for H_2S/H_2 pressure ratios < 0.05 reflecting realistic reaction conditions, the two non-equivalent sheets are both terminated by sulfur, one sulfur atom per surface molybdenum, however, with the surface sulfur positioned differently. Compared with the ideal surface this sulfur reconstructed geometry (Fig. 1b) corresponds to sulfur addition at the initial Mo terminated sheet (denoted T_1 termination) and sulfur depletion at the S terminated sheet (denoted T_2 termination). Lauritsen et al. [37] observed C_4H_7S species adsorbed at the brim edge of triangular MoS_2 nanoclusters by scanning tunneling microscopy (STM) and concluded that the brim edge is a new

kind of active site for HDS. However, so far there is no experimental evidence to indicate that CO hydrogenation can also occur at this brim edge. Triangular MoS_2 nanoclusters observed by Lauritsen exist usually under H_2S rich conditions during the HDS process which is not considered in this work.

The T_1 and T_2 terminated sheets, including adsorption of reaction intermediates, are examined in separate calculations where supercell model systems with only one sheet termination are used. Here slabs of identical sheets, either T_1 or T_2 terminated, containing four rows of molybdenum atoms and corresponding rows of sulfur atoms in each slab (Fig. 2a, b) are placed periodically with a separation of 10 Å of vacuum along the (0001) direction. The slabs are repeated periodically along the surface normal (equal to the (10-10) direction) with a vacuum separation of 10 Å between them. Test calculations confirmed that the chosen separation was sufficient to avoid electronic coupling between adjacent slabs. Theoretical studies for the T_1 model system have shown [28] that for low H_2S/H_2 pressure ratios the surface can become more stable thermodynamically if the sulfur concentration at the top is smaller than one S atom per underlying Mo atom. This can be achieved by including surface sulfur vacancies (leaving coordinatively unsaturated molybdenum surface sites) where, assuming H_2S/H_2 pressure ratios below 0.001, a reasonable value is one vacancy per six surface sulfur atoms corresponding to 42% relative S coverage (100% S coverage corresponds two surface S atoms per Mo atom [33]) at the real MoS_2(10-10) surface as sketched in Figs. 1b, 2a. [28] This model geometry, labeled T_1', is described by a sheet supercell with six MoS_x units along the surface edge and will be considered in the following. Adsorption of reaction intermediates at the sheet edges of the T_1' and T_2 model systems is considered in corresponding geometry optimizations where the adsorbates and the top-most substrate layers are allowed to relax freely while the two bottom layers of the slabs (Fig. 2) are fixed at the geometry of bulk MoS_2.

The electronic structure and equilibrium geometries of the model systems are calculated using the DMol^3 program package [38,39] where the generalized gradient corrected functional according to Perdew and Wang (PW91) is employed [40,41]. Extended numerical all-electron basis sets (double-zeta plus polarization, DNP) are used to describe the electronic structure of all atoms in the model systems except molybdenum where the 28-electron core is approximated by an effective core potential (ECP) [42,43] and a DNP basis is used to account for the valence electron structure. All electronic states are determined by calculations including spin polarization for the open shell species

in gas phase and for appropriate multiplet states of the adsorption systems. As a result of the large supercells the k point integration during the electronic structure calculations is restricted to one k point in the Brillouin zone. Geometry optimizations are performed with a numerical displacement accuracy of the atom centers of 5×10^{-3} Å. Possible transition states (TS) are located by using the complete linear and quadratic synchronous transit (LST, QST) method [44] connecting the most stable reactants and products. Corresponding adsorption energies, E_{ads}, are computed from appropriate differences of total energies of supercells of the MoS_2 slabs with adsorbates in their equilibrium geometries, E_{tot}(slab/ads), of the pure MoS_2 slabs, E_{tot}(slab), and of the free adsorbates in gas phase, E_{tot}(ads), i.e. by

$$E_{ads} = E_{tot}(\text{slab/ads}) - E_{tot}(\text{slab}) - E_{tot}(\text{ads}) \quad (3)$$

where negative E_{ads} values correspond to exothermic adsorption while positive E_{ads} means endothermic adsorption. The adsorption energies (3) are evaluated using total energies E_{tot}(ads) of the gas phase species in their neutral ground states. This is justified since the corresponding experiments have been carried out at T = 500-700 K where there is no solvent to provide charges. However, the corresponding adsorbates may become charged at the surface as a result of charge transfer which is accounted for by the selfconsistent treatment of the combined adsorbate-substrate system (slab/ads) in its neutral state.

The present calculations consider periodic slabs where the molecular adsorbates and reactants are added only on one side of the slab. This yields a non-symmetric slab system where in strongly polar systems charge rearrangements may result in large dipole contributions affecting the accuracy of the adsorption energies E_{ads}. This was studied in test calculations for the adsorption of formyl, **CHO** and formate, HCOO, at the T_1' terminated MoS_2 surface employing the Vienna Ab Initio Simulation Package (VASP) [45,46] (The DMol^3 code does not allow including dipole corrections in a straightforward way.) Dipole corrections were found to contribute to E_{ads} less than 0.04 eV for **CHO** and 0.05 eV for **HCOO**, respectively (2% of E_{ads} in both cases) which suggests strongly that these corrections can be ignored for the present purpose. The non-symmetric slab system has also been successfully applied by other groups using the DMol^3 code in theoretical studies on CO, H_2 adsorption, surface properties, and surface reactions at MoS_2 surfaces [28,35,36,47]. As specific examples, we mention work by Todorova et al. [47] on the hydrogenolysis reaction of CH_3SH to

CH_4 at the MoS_2(10-10) surface and by Huang et al. [35] on CO hydrogenation at prefect MoS_2(10-10) corresponding to our T_1 model.

In addition to geometric and energetic quantities, adsorbate charges *q* are determined by Mulliken charges summed over all atoms of the adsorbates. (It should be emphasized that all adsorbate charges based on Mulliken populations can be considered only as qualitative guidelines and not taken as quantitative entities of chemical relevance. In particular, they cannot represent formal valence charges.) Further, vibrational frequencies of the adsorbates are calculated following the harmonic approach using Hessian matrices where all substrate centers are fixed and only intra-adsorbate displacements are considered.

The calculations include reactions of the different intermediates of CO hydrogenation at the MoS_2(10-10) surface. For a reaction A + B → AB we define two different reaction scenarios. First we consider two separate species A, B at the surface which approach and react to form the product AB. This is described by a reaction energy ΔE_{sep} with

$$\Delta E_{sep} = [E_{tot}(slab/AB) + E_{tot}(slab)] - [E_{tot}(slab/A) + E_{tot}(slab/B)], \quad (4)$$

where E_{tot} are total energies (per unit cell) of the corresponding systems. Second, we consider the two species A, B in a coadsorption geometry where they stabilize at nearby sites followed by a reaction to form AB. This is described by a reaction energy ΔE_{coad} with

$$\Delta E_{coad} = E_{tot}(slab/AB) - E_{tot}(slab/(A+B)_{coad}) \quad . \quad (5)$$

where $E_{tot}(slab/(A+B)_{coad})$ denotes the total energy of the coadsorption system. Obviously, the difference ($\Delta E_{coad} - \Delta E_{sep}$) characterizes the interaction between A and B in the coadsorbed state at the surface with negative values for attraction and positive ones for repulsion. In Sec. 3, we will focus on the discussion of results for ΔE_{coad}.

3. RESULTS AND DISCUSSION

3.1. Adsorption of reaction intermediates

Table 1 lists the computed adsorption energies E_{ads} and adsorbate charges *q* of 16 possible intermediates occurring in CO hydrogenation reactions discussed above where stabilization at T_1' and T_2 terminated MoS_2 model surfaces is considered. As mentioned above, adsorption energies are evaluated using total energies E_{tot}(ads) of the gas phase species in their neutral ground states where charging like in the presence of a solvent is excluded. In addition, Figs. 3, 4 and 5 show the corresponding equilibrium geometries of the intermediates for both terminations. Here only adsorbate sites and geometries with largest E_{ads} are included while many more have been evaluated. In addition, for T_1' terminated MoS_2 we focus only on adsorption near the coordinatively unsaturated molybdenum surface site which is well accepted to play a major role in the adsorption and activation of the reactants [48−50]. All intermediate adsorbates stabilize at T_1' and T_2 terminated MoS_2 surfaces resulting in basically two different adsorption geometries where the adsorbate is bound to either one or two molybdenum centers as will be discussed in the following.

3.1.1. Adsorbed $C_1H_xO_y$ species

Extended optimizations of formyl, **CHO**, at the MoS_2 model surface yield for T_1' and T_2 termination three different local energy minima each where those of the most stable states for each termination are shown by their equilibrium geometries in Fig. 3a. Here the CO part is always found to bridge two adjacent molybdenum centers resulting in E_{ads} of -2.01 eV (T_1') and -1.98 eV (T_2) (Table 1a). Further, the C-O bond of the adsorbate is activated compared with free CHO increasing its C-O bond length from 1.19 Å to 1.25 (T_1') and 1.26 Å (T_2), respectively. Such C-O distance increase has also been obtained for COH, CH_2O, CH_3O, CHOH and CH_2OH (see below), where the effect is smallest for COH adsorbed at T_2 terminated MoS_2. The latter is explained by the fact that the adsorbate binds only with its carbon end to one Mo substrate atom (Fig. 3b), affecting the C-O bond only little. For hydroxy carbine, **COH**, two different local energy minima are obtained for T_1' and one for T_2 terminated MoS_2 surface. Here the most stable adsorbate geometry for T_1' yields the carbon end of the adsorbate binding to two adjacent 5-fold coordinated molybdenum centers (Fig. 3b top), while at T_2 termination the carbon end binds only with one Mo center. Consequently, the corresponding E_{ads} differ substantially, -3.49 eV for T_1' and -2.71 eV for T_2; revealing that COH prefers adsorption at T_1' terminated MoS_2 surface over T_2.

Geometry optimizations hydroxy methine, **CHOH**, at the MoS_2 model surface yield for T_1' and T_2 termination two different local energy minima each where those of lowest total energy for each termination are shown by their equilibrium geometries (Fig. 3c). In both cases the adsorbate is found to bridge two adjacent molybdenum centers with its carbon center which accounts for E_{ads} of -2.60 eV (T_1') and -2.61 eV (T_2) (Table 1a). This indicates very similar adsorbate binding for both surface terminations. The most stable adsorption geometries of the formaldehyde species, **CH_2O**, at the two differently terminated MoS_2 surfaces (of three local equilibrium geometries found for each termination) are sketched in Fig. 3d. While the E_{ads} at both sites are almost identical, -0.50 eV (T_1') and -0.52 eV (T_2) (Table 1a), the binding mechanisms are rather different. For T_1' termination the CO part of the adsorbate bridges two adjacent molybdenum centers whereas at T_2 terminated surface the molecule binds with its CO part to only one center yielding a 6-fold coordinated Mo species. The calculated E_{ads} value for CH_2O is found to be the smallest amongst all $C_1H_xO_y$ species considered. In addition, the adsorbate charge of CH_2O is very close to zero (Table 1), yielding an almost neutral species. These results are obvious since CH_2O forms a stable closed-shell molecule interacting more weakly with the substrate compared with the other $C_1H_xO_y$ species which represent highly reactive species. Weak adsorptive binding of CH_2O has also been observed on other substrates like e. g. the Pt(111) surface [51].

The most stable adsorption geometries of hydroxy methylen, **CH_2OH**, at the two MoS_2 surfaces (of two local equilibrium geometries found for each termination) are sketched in Fig. 3e. Here the adsorbate binding geometry is rather similar with the case of CH_2O. For T_1' termination the CO part of the adsorbate bridges two adjacent molybdenum centers whereas at T_2 terminated surface the molecule binds with its CO part to only one center yielding a 6-fold coordinated Mo species. The calculations yield E_{ads} of -1.99 eV (T_1') and -1.53 eV (T_2) (Table 1a), suggesting stronger binding for T_1' compared with T_2 termination.

Methoxy, **CH_3O**, stabilizes at T_1' and T_2 terminated MoS_2 surfaces with most favorable adsorption geometries that are similar. Here the oxygen end of the adsorbate binds between two adjacent molybdenum centers (Fig. 3f, two local equilibrium geometries for each termination are found). As for CH_2OH, binding is weaker at T_2 compared with T_1' terminated surface yielding E_{ads} of -3.20 eV (T_1') and -2.67 eV (T_2), respectively. Adsorption of formate, **HCOO**, and carbonate, **CO_3**, species, although not appearing in reaction steps (1) and (2a-c), is also considered for completeness.

Both species result in most stable adsorption geometries with oxygen of the corresponding OCO part bridging two adjacent molybdenum centers of the substrate, independent of the termination (Fig. 4a, b). The E_{ads} for HCOO, -2.95 eV (T_1') and -2.90 eV (T_2), differ only slightly between the terminations while for CO_3 the difference between the E_{ads} values, -3.95 eV (T_1') and -4.25 eV (T_2), is larger, suggesting weaker binding for T_1' compared with T_2 termination. The E_{ads} for CO_3 is the largest amongst all adsorbates considered in this study. This shows that this adsorbate is very strongly binding with the substrate where ionic contributions become important. The latter is confirmed by the relatively large negative charge of -0.6 to -0.7 calculated for the adsorbate (Table 1). Interestingly, the two C-O distances of the OCO part, common to both adsorbates, are not changed by the adsorption (i.e. distance differences are below 0.01 Å). This suggests that the OCO part is almost inert and cannot be activated easily.

3.1.2. Adsorbed $C_2H_xO_y$ species

Geometry optimizations of acetyl, **CH_3CO**, at the MoS_2 model surface yield for T_1' and T_2 termination two different local energy minima each where those of lowest total energy for each termination are shown by their equilibrium geometries in Fig. 4c. In both cases the CO part of the adsorbate is found to bridge two adjacent molybdenum centers resulting in E_{ads} of -1.98 eV (T_1') and -2.03 eV (T_2) (Table 1b), indicating very similar adsorbate binding for both surface terminations. For both terminations the C-O distance of free CH_3CO is increased from 1.19 to 1.25 Å in the adsorbed state which can be understood as an adsorption-induced activation of the C-O bond in CH_3CO. The most stable adsorption geometries of acetaldehyde, **CH_3CHO**, at the two differently terminated MoS_2 surfaces are shown in Fig. 4d. Obviously, the resulting binding scheme is similar in both cases: CH_3CHO binds with its oxygen tail at one molybdenum center. This yields quite small E_{ads} of -0.40 eV (T_1') and -0.34 eV (T_2) (Table 1b), which are the smallest amongst all $C_2H_xO_y$ species considered in the present work. This is, in analogy with the previous result for CH_2O, explained by CH_3CHO forming a stable closed-shell molecule which, therefore, interacts weakly with the substrate. The C-O distance in free CH_3CHO is increased by only 0.02 Å due to adsorption at T_1' or T_2 terminated surface. This can be understood, analogous to the findings for COH, by the fact that CH_3CHO binds only with its carbon end to one Mo substrate atom (Fig. 4d), influencing the

C-O bond only little. CH_3CHO species has been identified by temperature programmed desorption (TPD) measurements in CO hydrogenation on Co/Cu-based catalyst [18,19].

Ethoxy, **CH_3CH_2O**, stabilizes at T_1' and T_2 terminated MoS_2 surfaces with most favorable adsorption geometries, are also similar. The oxygen tail of the adsorbate binds in both cases between two adjacent molybdenum centers (Fig. 4e). Here binding is stronger at T_1' compared with T_2 terminated surface with E_{ads} of -3.16 eV (T_1') and -2.67 eV (T_2), respectively. Finally, acetate, **CH_3COO**, leads to most stable adsorption geometries with oxygen of the corresponding OCO part bridging two adjacent molybdenum centers of the substrate, independent of the termination (Fig. 4f). The E_{ads} amount to -2.87 eV (T_1') and -2.73 eV (T_2), respectively, which yields a slight energetic preference for T_1' termination of the MoS_2 surface. As for HCOO and CO_3 discussed above, the two C-O distances of the OCO part of CH_3COO are not affected by adsorption suggesting that the OCO part of the adsorbate cannot be activated easily.

3.1.3. Adsorbed CH_x and OH_x species

Atomic **carbon** was found to adsorb at both the T_1' and T_2 terminated MoS_2 surfaces bridging two adjacent molybdenum centers and coupling with the nearest sulfur center, see Fig. 5a, and forming fairly strong bonds as indicated by E_{ads} values of -5.40 (T_1') and -5.56 eV (T_2). Both **CH** and **CH_2** adsorbates exhibit the most stable adsorption geometries also with carbon bridging two adjacent molybdenum sites by strong adsorption bonds, see Fig. 5b, c. In addition, CH couples with the nearest sulfur center, analogous to atomic carbon, whereas CH_2 binds only with molybdenum centers. The computed adsorption energies E_{ads} are -5.73 (T_1') and -6.03 eV (T_2) for CH while they amount to -4.26 (T_1') and -4.41 eV (T_2) for CH_2. The most stable adsorbate geometry for **CH_3** yields the carbon end of the adsorbate binding to only one molybdenum center such that the carbon is 4-fold coordinated in a distorted tetrahedral environment, see Fig. 5d. In this geometry the adsorption bond is relatively weak leading to E_{ads} values of -1.71 (T_1') and -1.59 eV (T_2), respectively. Finally, atomic **oxygen** and **OH** are also found to stabilize at both the T_1' and T_2 terminated MoS_2 surfaces where the oxygen bridges two adjacent molybdenum centers. The computed adsorption energies E_{ads} amount to -5.43 (T_1') and -5.17 eV (T_2), respectively, for atomic oxygen and to -3.86 (T_1') and -3.49 eV (T_2) for OH.

3.2. Vibrational properties of reaction intermediates

Koizumi et al. [8] examined CO hydrogenation at unpromoted MoS_2/γ-Al_2O_3 catalysts using in situ DRIFT spectroscopy and observed six different peaks at 2060 cm^{-1}, 2010 cm^{-1}, 1590 cm^{-1}, 1470 cm^{-1}, 1420 cm^{-1}, and 1385 cm^{-1}. The peaks at 2060 cm^{-1} and 2010 cm^{-1} were attributed to CO adsorption and also confirmed by separate experiments and calculations [32]. Here we restrict ourselves to the peak region between 1280 and 1600 cm^{-1} ignoring CH_x and OH vibrations which lie outside this frequency range. All the other reaction intermediates are examined in their vibrational behavior by corresponding normal mode analyses in the adsorbed state. Characteristic frequencies for each adsorbate at the T_1' and T_2 terminated MoS_2(10-10) surfaces are listed in Table 2 where the calculated values are restricted to a range between 1280 and 1600 cm^{-1} reflecting the experimental range considered in the DRIFT experiments for an MoS_2/γ-Al_2O_3 catalyst [8]. In addition, Table 3 compares the computed vibrational frequencies of the adsorbates with the experimental DRIFT data [8] where vibrations of the different adsorbates in a given frequency range are combined for the comparison with experimental peaks (given by their peak center). The comparison confirms most of the experimental assignments by theory but yield also additional information from the calculations.

The calculations yield vibrations for the four adsorbates CHOH, COH, CHO and CH_3CO in the frequency range between 1286 and 1336 cm^{-1} which could explain the rather weak structure in the experimental infrared spectrum slightly above 1300 cm^{-1}. Further, the experimental spectrum shows two broadened peaks with additional structure between 1370 and 1400 cm^{-1} where the peak at lower frequency near 1385 cm^{-1} was assigned [8] to formate, HCOO, while the higher peak was not identified. In the calculations the frequency region between 1349 and 1403 cm^{-1} accommodates vibrational excitations from five different adsorbates listed in Table 3. This includes HCOO at 1374 (T_1') and 1372 cm^{-1} (T_2) (Table 2), which is consistent with the previous interpretation of the experimental lower peak. In addition, the higher experimental peak near 1395 cm^{-1} is assigned in the calculations to a combination of the four CH_3 containing adsorbates CH_3CO, CH_3CHO, CH_3COO and CH_3CH_2O where the relative importance of the difference species can be determined only in separate experiments.

There is an additional structure between 1415 and 1440 cm^{-1} in the experimental spectrum

where lower end at 1420 cm^{-1} was assigned [8] also to HCOO. The latter cannot be confirmed by the present calculations. The experimental frequency range between 1413 and 1443 cm^{-1} is described in the calculations by vibrations of the six CH_2 and CH_3 containing adsorbates CH_2O, CH_2OH, CH_3O, CH_3CO, CH_3CHO and CH_3COO (Table 3), with no contribution from formate. The peak region near 1470 cm^{-1} in the experimental spectrum was assigned [8] to vibrations of the three adsorbates CH_3COO, CH_3O and CO_3. This is only partly compatible with our computed results where the experimental frequency range between 1447 and 1488 cm^{-1} is covered by vibrations of the six adsorbates CH_3COO, CH_3O, CHO, COH, CH_3CO and CH_3CH_2O (Table 3), with CO_3 missing. Instead, vibrations of adsorbed CO_3 are calculated to yield frequencies of 1747 cm^{-1} (T_1') and 1744 cm^{-1} (T_2) (Table 2), where there is no clear structure in the experimental spectrum. This may indicate that carbonate species do not appear in the CO hydrogenation experiment under the conditions described in Ref. [8] (Note that vibrations of adsorbed bridging CO_3 on Pt catalysts have been measured to yield 1725 cm^{-1} [52].) Finally, the experimental spectrum shows a broad asymmetric peak between 1560 and 1600 cm^{-1} where a frequency of 1590 cm^{-1} was assigned [8] to vibrations of the HCOO. This is confirmed by the calculations which yield HCOO vibrations at 1535 and 1562 cm^{-1} giving further evidence that the formate adsorbate appears in the CO hydrogenation experiment described in Ref. [8].

3.3. CO hydrogenation at the MoS_2 surface

CO hydrogenation on pure MoS_2 is found to yield mainly C_1 type products. Therefore, we focus in the following on reaction steps producing C_1 species. Corresponding reaction energies, ΔE_{coad} and ΔE_{sep}, as well as activation energies E_a, involving all reaction intermediates discussed in Sec. 3.1 have been evaluated and are listed in Table 4. Figs. 6, 7 sketch calculated geometric structures of the optimized reactants, transition states, and products at the T_1' and T_2 terminated MoS_2 surfaces for the most favorable reaction paths each. Further, Fig. 8 shows corresponding energetic reaction schemes based on the results of Table 4 where the most favorable reaction path is highlighted by thick lines. Overall, the results in Table 4 show that reaction energies starting from completely separated surface species, ΔE_{sep} of definition (4), and from coadsorbed nearby species, ΔE_{coad} of definition (5), yield the same trends. (The same conclusions have been arrived at in studies on the

dehydrogenation of methanol over Pt (111) surface [51].) They quantify thermodynamic reaction properties and are used in the following to characterize relative thermodynamic reaction probabilities (only ΔE_{coad} values will be mentioned). In contrast, the energy barriers E_a, given in Table 4 and discussed in the following, characterize kinetic probabilities of corresponding reactions. It should be emphasized that our reaction studies are always based on Langmuir-Hinshelwood [53] type reaction schemes (which may also be connected with hydrogen spillover [28,31]) where only adsorbed species are considered and additional adsorption/desorption processes are ignored.

3.3.1. Initial reaction of CO with hydrogen

Fig. 6a shows that coadsorption of CO and H at the T_1' terminated MoS_2 edge yields CO adsorbed near the 5-fold Mo site with H at the nearby top S site. Starting from this coadsorption, CHO formation is more favorable than COH both kinetically (E_a = 1.45 vs. 1.75 eV) and thermodynamically (ΔE_{coad} = 0.36 vs. 0.79 eV), see Table 4. Subsequent dissociation of adsorbed CHO to yield CH and O is connected with a barrier of 1.46 eV and is endothermic by 0.80 eV. Obviously, CHO will be the first intermediate of CO reacting with hydrogen. The same qualitative results, with, however, larger barriers are found for the T_2 terminated MoS_2 edge, see Fig. 7a.

The CHO adsorbate may react with another hydrogen adsorbate to form CH_2O or CHOH surface species. The coadsorbate geometry at the T_1' terminated MoS_2 edge yields CHO assuming the geometry of the previous hydrogenation reaction and the hydrogen stabilizing at a nearby top S site, either close to the carbon or close to the oxygen of the CHO adsorbate. While two coadsorbate configurations are close in energy the first geometry leads to CH_2O as a reaction product as shown in Fig. 6b while the latter results in CHOH. Here CH_2O formation is more favorable than CHOH both kinetically (E_a = 0.79 vs. 1.06 eV) and thermodynamically (ΔE_{coad} = -0.48 vs. 0.00 eV). Subsequent dissociation of adsorbed CH_2O into CH_2 and O is connected with a barrier of 1.47 eV and is exothermic by -0.28 eV. The same qualitative results, with, however, larger barriers are found for the T_2 terminated MoS_2 edge, see Fig. 7b. Thus the second intermediate for CO hydrogenation will be CH_2O.

The CH_2O adsorbate can react with another hydrogen adsorbate to form CH_2OH or CH_3O

surface species. As before the coadsorbate geometry at the T_1' terminated MoS_2 edge allows for hydrogen stabilizing at a top S site, either close to the carbon or close to the oxygen of the CH_2O adsorbate where the two configurations are close in energy. Here the first geometry leads to CH_3O as a reaction product as illustrated in Fig. 6c while the latter results in CH_2OH. The numerical results in Table 4 show that both CH_2OH and CH_3O formation are favorable thermodynamically (ΔE_{coad} = -0.52 vs. -1.36 eV) where the former is kinetically more favorable (E_a = 0.88 vs. 1.60 eV). Subsequent dissociation of adsorbed CH_2OH into CH_2 and OH is connected with a barrier of 0.95 eV and is exothermic by -0.29 eV. On the other hand, CH_3O dissociation into surface CH_3 and O is neither kinetically (E_a = 2.59 eV) nor thermodynamically feasible (ΔE_{coad} = 1.35 eV). Altogether, the dissociation of adsorbed CH_2OH into CH_2 and OH is more likely to happen. As another competing step, CH_2OH may react with surface hydrogen to form CH_3OH. However, our calculations show that the hydrogenation of CH_2OH, while gaining more energy than the dissociation, is less likely to occur due to its reaction barrier, 1.26 eV, see Table 4, which is higher than that of the dissociation process, 0.95 eV. Qualitatively similar results are found for the T_2 terminated MoS_2 edge, see Fig. 7c. Thus the third intermediate for CO hydrogenation will be CH_2OH followed by cleavage of its C-O bond.

3.3.2. Reaction of CH_2 with hydrogen

As discussed above, CO hydrogenation at the MoS_2(10-10) surface will yield, amongst other products, surface CH_2. This species can react further with adsorbed hydrogen yielding CH_4 in two reaction steps. The coadsorbate geometry at the T_1' edge yields CH_2 bridging two Mo centers and the hydrogen stabilizing at a nearby top S site. This leads to adsorbed CH_3 as a reaction product as shown in Fig. 6d where the reaction is exothermic (ΔE_{coad} = -0.20 eV) and connected with a moderate barrier of E_a = 0.97 eV. In a subsequent reaction the adsorbed CH_3 can combine with another hydrogen to produce CH_4 where the reaction is strongly exothermic (ΔE_{coad} = -1.26 eV) and connected with a barrier of only E_a = 0.53 eV. For comparison, adsorbed CH_3 reacting with surface OH to form CH_3OH is found to yield a rather high barrier, E_a = 1.68 eV, and is much less exothermic, ΔE_{coad} = -0.38 eV, than CH_4 formation. The same qualitative results are found for the T_2 terminated MoS_2 edge, see Fig. 7d. Altogether, the calculations show that CH_2 reacting with hydrogen at the MoS_2(10-10) surface to form adsorbed CH_4 is a very likely process. The resulting CH_4 species can

be assumed to bind very weakly with the surface and may easily desorb.

3.3.3. Optimized reaction paths

Fig. 8 shows energetic reaction schemes for sequential CO hydrogenation at the MoS_2(10-10) surface for both T_1' (Fig. 8a) and T_2 edges (Fig. 8b) which consider all reaction steps discussed above where reaction intermediates and products are assumed in their adsorbed states at the surface resulting in Langmuir-Hinshelwood type reactions. This yields optimized reaction paths combining energetically lowest reaction intermediates and lowest reaction barriers which are highlighted by thick lines in Fig.8. Obviously, the most favorable reaction path is qualitatively the same for both terminations and involves C_1 type surface species in the sequence

$$CO \rightarrow CHO \rightarrow CH_2O \rightarrow CH_2OH \rightarrow CH_2 \rightarrow CH_3 \rightarrow CH_4 \qquad (6)$$

This pathway is consistent with experimental findings [8] but disagrees in some details with recent theoretical studies [35] where the MoS_2(10-10) surface was modeled with pure Mo metal and pure sulfur termination. The authors find for the pure Mo metal termination that both adsorbed CHO and CH_2O species can dissociate breaking its C-O bond in an exothermic reaction with a rather low barrier. (The corresponding E_a and ΔE_{coad} values are included in Table 4.) This misses the reaction intermediates CH_2OH and CH_3O found in the present study and leads to a shortened reaction path which involves C_1 type surface species in the sequence

$$CO \rightarrow CHO \rightarrow CH_2O \rightarrow CH_3 \rightarrow CH_4 \quad . \qquad (7)$$

The discrepancy is most likely due to the different MoS_2 surface terminations considered Ref. [35] as compared to the present study where the present surface terminations are believed to be more realistic. It should be noted that on both the sulfur covered and the pure metal surface, formyl (CHO) is the first intermediate for the activation of CO. Surface formyl is also found as the most important intermediate in Fischer-Tropsch process on metal surfaces [54] and in the reforming of CO_2 to methane on Ni surfaces [55].

4. CONCLUSIONS

The present theoretical studies give a clear account of the adsorption of reaction intermediates appearing during CO hydrogenation at the sulfur covered MoS_2(10-10) surface as well as of the elementary reaction steps. Periodic density functional theory calculations using the generalized gradient corrected functional due to Perdew and Wang [40,41] provide adsorption energies of the different adsorbates. The results, considering two different surface terminations of MoS_2(10-10), show highly localized strong adsorbate - molybdenum interaction for all (slightly charged) adsorbates with adsorption energies ranging between -1.6 eV and -6.0 eV. Adsorption of the (neutral) molecular reaction intermediates CH_2O and CH_3CHO is found to be much weaker yielding adsorption energies E_{ads} of -0.5 eV and -0.4 eV, respectively.

The reaction intermediates $C_1H_xO_y$ and $C_2H_xO_y$ are examined in their vibrational behavior by corresponding normal mode analyses in the adsorbed state. A comparison of the computed vibrational frequencies with experimental data from measurements applying infrared (DRIFT) spectroscopy to a MoS_2/γ-Al_2O_3 catalyst [8] confirms most of the experimental assignments but yields also new information. In particular, the frequency analyses give clear evidence that formate species, HCOO, appears in the CO hydrogenation experiment under the conditions described in Ref. [8] while they suggest that carbonate species, CO_3, may not participate in the reaction. More detailed information can be obtained only after experimental spectra with higher resolution have been carried out in CO hydrogenation experiments under well defined conditions where additional measurements are performed to identify possible reaction intermediates.

Further, systematic density-functional theory studies on possible reaction steps during CO hydrogenation at the sulfur covered MoS_2(10-10) surface are used to identify optimized reaction paths which are found to involve C_1 type surface species in the sequence

$$CO \rightarrow CHO \rightarrow CH_2O \rightarrow CH_2OH \rightarrow CH_2 \rightarrow CH_3 \rightarrow CH_4 \quad .$$

In particular, the dissociation of adsorbed CH_2OH results in CH_2 and OH products where CH_2 can react further to form CH_4. In addition, surface OH formed during the reactions may dissociate into adsorbed O and H or react with hydrogen to form water species undergoing a water-gas-shift reaction. These processes merit a separate discussion which goes beyond the scope of the present work

and will be considered in a subsequent study. The above pathway is consistent with experimental findings [8] but disagrees in some details with recent theoretical studies [35] where the MoS_2(10-10) surface was modeled with pure Mo metal and pure sulfur termination. The disagreement is most likely due to differences in the MoS_2 surface terminations considered in the studies. The present results cannot confirm the existence of formate, HCOO, intermediates found in the experiment [8]. This may be explained by the fact that in CO hydrogenation experiments on MoS_2 catalysts there is always a high probability of the water-gas shift reaction, $CO + H_2O \rightarrow H_2 + CO_2$, occurring in parallel. The latter is bond to produce formate as a reaction intermediate [56−60] which was discussed elsewhere [61].

ACKNOWLEDGEMENTS

This work was partly supported by the National Natural Science Foundation of China (No. 20590363 and 20876163), by the State Key Fundamental Research Program (No. 2007CB216401), and by the Deutsche Forschungsgemeinschaft (DFG) through its Collaborative Research Center SFB 546 (Transition metal oxide aggregates). One of the authors (X. S.) acknowledges financial support by the Max-Planck Society. We thank Jia Hu, Wenjuan Zhang and Lili Bao in our group for technical support.

Table 1. Adsorption energies E_{ads} (in eV) and adsorbate charges *q* (in atomic units) of all reaction intermediates at the MoS_2(10-10) surface considered in this work. The data are listed for both the T_1' and T_2 termination. Corresponding adsorption geometries are shown in Figs. 3, 4.

	$E_{ads}(T_1')$ / $E_{ads}(T_2)$	$q(T_1')$ / $q(T_2)$
$C_1H_xO_y$ and CO_3 species		
CHO	-2.01 / -1.98	0.11 / 0.14
COH	-3.49 / -2.71	0.22 / 0.44
CHOH	-2.60 / -2.61	0.20 / 0.16
CH_2O	-0.50 / -0.52	-0.06 / -0.01
CH_2OH	-1.99 / -1.53	0.17 / 0.17
CH_3O	-3.20 / -2.67	-0.20 / -0.18
HCOO	-2.95 / -2.90	-0.21 / -0.23
CO_3	-3.95 / -4.25	-0.62 / -0.67
$C_2H_xO_y$ species		
CH_3CO	-1.98 / -2.03	0.18 / 0.18
CH_3CHO	-0.40 / -0.34	0.23 / 0.21
CH_3CH_2O	-3.16 / -2.67	-0.16 / -0.16
CH_3COO	-2.87 / -2.73	-0.16 / -0.18
CH_x species		
C	-5.40 / -5.56	0.07 / 0.09
CH	-5.73 / -6.03	0.10 / 0.10
CH_2	-4.26 / -4.41	0.10 / 0.15
CH_3	-1.71 / -1.59	0.24 / 0.29

Table 2. Vibrational frequencies ν (in cm^{-1}) of all reaction intermediates at the MoS_2(10-10) surface considered in this work. The data are listed for both the T_1' and T_2 termination. The corresponding adsorption geometries are shown in Figs. 3, 4.

	ν(T_1')	ν(T_2)
CHO	1336, 1488	1310, 1483
COH	1298	1468
CHOH	1286	1317
CH_2O	1418	1422
CH_2OH	1424	1437
CH_3O	1421, 1440, 1465	1420, 1443, 1455
HCOO	1355, 1374, 1535	1358, 1372, 1562
CO_3	1747	1744
CH_3CO	1327, 1386, 1434, 1467	1329, 1419, 1450, 1517
CH_3CHO	1349, 1391, 1423, 1441	1373, 1383, 1431, 1442
CH_3CH_2O	1373, 1392, 1454, 1466, 1476	1357, 1381, 1450, 1458, 1485
CH_3COO	1379, 1413, 1439, 1448, 1534	1356, 1403, 1442, 1447, 1531

Table 3. Comparison of the computed vibrational frequencies ν (in cm^{-1}) of reaction intermediates adsorbed at the MoS_2(10-10) surface with experimental data from DRIFT spectroscopy for CO hydrogenation at the unpromoted MoS_2/γ-Al_2O_3 catalyst [8].

Theory		Experiment	
ν [cm^{-1}]	Assignment	ν	Assignment
[1286, 1336]	CHOH, COH (T_1'), CHO, CH_3CO	--	--
[1349, 1403]	HCOO, CH_3CO (T_1'), CH_3CHO, CH_3COO, CH_3CH_2O	1385	HCOO
[1413, 1443]	CH_2O, CH_2OH, CH_3O, CH_3CO, CH_3CHO, CH_3COO	1420	HCOO
[1447, 1488]	CH_3COO, CH_3O, CHO, COH (T_2), CH_3CO, CH_3CH_2O	1470	CH_3COO, CH_3O, CO_3
[1535, 1562]	HCOO	1590	HCOO
[1744, 1747]	CO_3	--	--

Table 4. Reaction energies, ΔE_{sep} and ΔE_{coad}, and reaction barriers, E_a, of different elementary steps for CO hydrogenation at the MoS_2(10-10) surface. For definitions of ΔE_{sep}, ΔE_{coad}, E_a, see text. All energies are given in eV. The numbers in parentheses refer to theoretical values for a pure Mo metal termination [35], also labeled with "a", see Fig. 1 and text.

Reaction step	T_1' termination			T_2 termination		
	ΔE_{sep}	ΔE_{coad}	E_a	ΔE_{sep}	ΔE_{coad}	E_a
CO + H						
CO + H → CHO	0.11	0.36 (0.51[a])	1.45	0.15	0.23	0.81
CO + H → COH	0.54	0.79 (1.71[a])	1.75	1.33	1.46	3.52
CHO → CH + O	0.21	0.80 (-0.69[a])	1.46 (0.50[a])	0.13	-0.23	2.53
CO + 2H						
CHO + H → CH_2O	-0.13	-0.48 (0.20[a])	0.79	-0.21	0.06	1.23
CHO + H → CHOH	0.36	0.00 (1.00[a])	1.06	0.28	0.64	1.73
CH_2O → CH_2 + O	0.04	-0.28 (-0.73[a])	1.47 (0.31[a])	0.17	0.02	1.87
CO + 3H						
CH_2O + H → CH_3O	-1.48	-1.36	1.60	-0.96	-0.84	1.43
CH_2O + H → CH_2OH	-0.65	-0.52	0.88	-0.20	-0.10	0.63
CH_3O → CH_3 + O	0.68	1.35	2.59	0.52	0.76	2.26
CH_2OH → CH_2 + OH	-0.32	-0.29	0.95	-0.47	-0.56	0.95
Misc						
CH_2OH + H → CH_3OH	-0.46	-0.78	1.26	-0.81	-0.62	1.60
CH_2 + H → CH_3	-0.84	-0.20 (-0.01[a])	0.97	-0.60	-0.57	0.79
CH_3 + H → CH_4	-0.70	-1.26 (0.42[a])	0.53 (0.58[a])	-0.86	-0.98	1.09
CH_3 + OH → CH_3OH	0.67	-0.38	1.68	0.26	0.32	3.57

FIGURE CAPTIONS

Fig. 1. Crystal structure of hexagonal MoS_2 at the (10-10) surface with (a) ideal bulk termination, (b) sulfur reconstructed termination, see text. Molybdenum (sulfur) centers are shown by small dark (large light) balls with connecting sticks visualizing atom coordination. The two differently Mo and S terminated layers are labeled accordingly.

Fig. 2. Slabs of (a) T_1' terminated, (b) T_2 terminated MoS_2 sheets used for the supercell model systems, see text. Molybdenum (sulfur) centers are shown by small dark (large light) balls with connecting sticks visualizing atom coordination. Vector R_s denotes the supercell periodicity along the sheet edge including six MoS_x units.

Fig. 3. Computed equilibrium geometries of selected C_1 reaction intermediates at T_1' and T_2 terminated edges of the MoS_2(10-10) surface, (a) CHO; (b) COH; (c) CHOH; (d) CH_2O; (e) CH_2OH; and (f) CH_3O. The atom centers are shown by shaded balls of different size and labeled in Fig. 3a. Connecting sticks are meant to visualize atom coordination.

Fig. 4. Computed equilibrium geometries of selected C_1 and C_2 type reaction intermediates at T_1' and T_2 terminated edges of the MoS_2(10-10) surface, (a) HCOO; (b) CO_3; (c) CH_3CO; (d) CH_3CHO; (e) CH_3CH_2O; (f) CH_3COO. The atom centers are shown by shaded balls of different size and labeled in Fig. 4a. Connecting sticks are meant to visualize atom coordination.

Fig. 5. Computed equilibrium geometries of selected CH_x species at T_1' and T_2 terminated edges of the MoS_2(10-10) surface, (a) C; (b) CH; (c) CH_2; (d) CH_3. The atom centers are shown by shaded balls of different size and labeled in Fig. 5a. Connecting sticks are meant to visualize atom coordination.

Fig. 6. Sequential CO hydrogenation steps at the T_1' edge for the most favorable reaction path: The structures to the left denote initial reactants, those on the right refer to products, and the center structures sketch corresponding transition states.

Fig. 7. Sequential CO hydrogenation steps at the T_2 edge for the most favorable reaction path: The structures to the left denote initial reactants, those on the right refer to products, and the center structures sketch corresponding transition states.

Fig. 8. Energetic reaction schemes for sequential CO hydrogenation at the (a) T_1' edge and (b) T_2 edge assuming reaction intermediates and products in their adsorbed states at the surface. The most favorable reaction paths are highlighted by thick lines. Alternative intermediates are labeled accordingly and listed at the bottom of the graph. The barriers between the reaction intermediates refer to corresponding reaction barriers.

REFERENCES

[1] M. Saito, R.B. Anderson, J. Catal. 63 (1980) 438.

[2] C.B. Murchison, M.M. Conway, R.R. Stevens, G.J. Guarderer, Proc. 9th Int. Congress on Catalysis 2 (1988) 626.

[3] J.S. Lee, S. Kim, K.H. Lee, I.S. Nam, J.S. Chung, Y.G. Kim, H.C. Woo, Appl. Catal. A 110 (1994) 11.

[4] Y. Xie, B.N. Naasz, G.A. Somorjai, Appl. Catal. 27 (1986) 233.

[5] J. Zhang, Y. Wang, L. Chang, Appl. Catal. A 126 (1995) L205.

[6] Y. Avila, C. Kappenstein, S. Pronier, J. Barrault, Appl. Catal. A 132 (1995) 97.

[7] Z.-R. Li, Y.-L. Fu, M. Jiang, T.-D. Hu, T. Liu, Y.-N. Xie, J. Catal. 199 (2001) 155.

[8] N. Koizumi, G. Bian, K. Murai, T. Ozaki, M. Yamada, J. Mol. Catal. A: Chem. 207 (2004) 173.

[9] Z. Li, Y. Fu, J. Bao, M. Jiang, T. Hu, T. Liu, Y. Xie, Appl. Catal. A 220 (2001) 21.

[10] D. Li, C.Yang, H. Qi, H. Zhang, W. Li, Y. Sun, B. Zhong, Catal. Commun. 5 (2004) 605.

[11] D. Li, C.Yang, W. Li, Y. Sun, B. Zhong, Top. Catal. 32 (2005) 233.

[12] R.G. Herman, Catal. Today 55 (2000) 233.

[13] T. Tatsumi, A. Muramatsu, K.Yokota, H. Tominaoa, J. Catal. 115 (1989) 388.

[14] S.C. Chuang, Y.H. Tian, J.G. Goodwin Jr., I. Wender, J. Catal. 96 (1985) 396.

[15] J.G. Numan, C.E. Bogdan, K. Kiler, K.J. Smith, C.-W. Young, R.G. Herman, J. Catal. 116 (1989) 195.

[16] T.Y. Park, I.-S. Nam, Y.G. Kim, Ind. Eng. Chem. Res. 36 (1997) 5246.

[17] J.G. Santiesteban, C.E. Bogdan, R.G. Herman, K. Klier, Proc. 9th Int. Congress on Catalysis 2 (1988) 561.

[18] A. Kiennemann, S. Boujana, C. Diagne, P. Chaumette, Stud. Surf. Sci. Catal. 75 (1993) 1479.

[19] A. Kiennemann, S. Boujana, C. Diagne, P. Courty, P. Chaumette, Stud. Surf. Sci. Catal. 61 (1991) 243.

[20] A. Travert, H. Nakamura, R.A. van Santen, S. Cristol, J.-F. Paul, E. Payen, J. Am. Chem. Soc. 124 (2002) 7084.

[21] Y.-W. Li, X.-Y. Pang, B. Delmon, J. Mol. Catal. A 169 (2001) 259.

[22] P. Faye, E. Payen, D. Bougeard, J. Catal. 179 (1998) 560.

[23] L.S. Byskov, J.K. Nørskov, B.S. Clausen, H. Topsøe, J. Catal. 187 (1999) 109.

[24] H. Schweiger, P. Raybaud, G. Kresse, H. Toulhoat, J. Catal. 207 (2002) 76.

[25] Á. Logadóttir, P.G. Moses, B. Hinnemann, N.-Y. Topsøe, K.G. Knudsen, H. Topsøe, J.K. Nørskov, Catal. Today 111 (2006) 44.

[26] V. Alexiev, R. Prins, T. Weber, Phys. Chem. Chem. Phys. 2 (2000) 1815.

[27] M.V. Bollinger, K.W. Jacobsen, J.K. Nørskov, Phys. Rev. B 67 (2003) 085410.

[28] M. Sun, A.E. Nelson, J. Adjaye, Catal. Today 105 (2005) 36.

[29] S. Cristol, J.F. Paul, E. Payen, J. Phys. Chem. B 106 (2002) 5659.

[30] (a) T. Zeng, X.-D. Wen, G.-S. Wu, Y.-W. Li, H. Jiao, J. Phys. Chem. B 109 (2005) 2846. (b) T. Zeng, X.-D. Wen, Y.-W. Li, H. Jiao, J. Phys. Chem. B 109 (2005) 13704. (c) T. Zeng, X.-D. Wen, Y.-W. Li, H. Jiao, J. Mol. Catal. A 241 (2005) 219. (d) X.-D. Wen, T. Zeng, H. Jiao, J. Phys. Chem. B 110 (2006) 14004.

[31] X.-D. Wen, T. Zeng, B.-T. Teng, F.-Q. Zhang, Y.-W. Li, J. Wang, H. Jiao, J. Mol. Catal. A 249 (2006) 191.

[32] A. Travert, C. Dujardin, F. Maugé, S. Cristol, J.-F. Paul, E. Payen, D. Bougeard, Catal. Today 70 (2001) 255.

[33] P. Raybaud, J. Hafner, G. Kresse, S. Kasztelan, H. Toulhoat, J. Catal. 189 (2000) 129.

[34] S. Cristol, J.F. Paul, E. Payen, D. Bougeard, S. Clémendot, F. Hutschka, J. Phys. Chem. B 104 (2000) 11220.

[35] M. Huang, K. Cho, J. Phys. Chem. C 113 (2009) 5238.

[36] M. Sun, J. Adjaye, A.E. Nelson, Appl. Catal. A 263 (2004) 131.

[37] J.V. Lauritsen, M. Nyberg, J.K. Nørskov, B.S. Clausen, H. Topsøe, E. Lægsgaard, F. Besenbacher, J. Catal. 224 (2004) 94.

[38] B. Delley, J. Chem. Phys. 92 (1990) 508.

[39] B. Delley, J. Chem. Phys. 113 (2000) 7756.

[40] J.P. Perdew, Y. Wang, Phys. Rev. B 45 (1992) 13244.

[41] J.P. Perdew, J.A. Chevary, S.H. Vosko, Phys. Rev. B 46 (1992) 6671.

[42] M. Dolg, U. Wedig, H. Stoll, H. Preuss, J. Chem. Phys. 86 (1987) 866.

[43] A. Bergner, M. Dolg, W. Kuechle, H. Stoll, H. Preuss, Mol. Phys. 80 (1993) 1431.

[44] T.A. Halgren, W.N. Lipscomb, Chem. Phys. Lett. 49 (1977) 225.

[45] G. Kresse, J. Furthmüller, Comput. Mater. Sci. 6 (1996) 15.

[46] G. Kresse, J. Furthmüller, Phys. Rev. B 54 (1996) 11169.

[47] T. Todorova, R. Prins, Th. Weber, J. Catal. 236 (2005) 190.

[48] B. Delmon, Bull. Soc. Chim. Belg. 88 (1979) 979.

[49] (a) X.-Q. Yao, Y.-W. Li, H. Jiao, J. Mol. Struct. (Theochem) 726 (2005) 67. (b) X.-Q. Yao, Y.-W. Li, H. Jiao, J. Mol. Struct. (Theochem) 726 (2005) 81.

[50] B. Delmon, G.F. Froment, Catal. Rev. Sci. Eng. 38 (1996) 69.

[51] S.K. Desai, M. Neurock, K. Kourtakis, J. Phys. Chem. B 106 (2002) 2559.

[52] G.R. Bamwenda, A. Ogata, A. Obuchi, J. Oi, K. Mizuno, J. Skrzypek, Appl. Catal. B 6 (1995) 311.

[53] C.N. Hinshelwood, Kinetics of Chemical Changes, Oxford, Clarendon Press, U.K. (1940) 197.

[54] (a) S.-G. Wang, D.-B. Cao, Y.-W. Li, J. Wang, H. Jiao, J. Phys. Chem. B 110 (2006) 9976. (b) C. Huo, J. Ren, Y. Li, J. Wang, H. Jiao, J. Catal. 249 (2007) 174. (c) O.R. Inderwildi, S.J. Jenkins, D.A. King, J. Phys. Chem. C 112 (2008) 1305. (d) C. Huo, Y. Li, J. Wang, H. Jiao, J. Phys. Chem. C 112 (2008) 14108. (e) O.R. Inderwildi, S.J. Jenkins, D.A. King, Angew. Chem. Int. Ed. 47 (2008) 5253.

[55] S.-G. Wang, X.-Y. Liao, J. Hu, D.-B. Cao, Y.-W. Li, J.G. Wang, H. Jiao, Surf. Sci. 601 (2007) 1271.

[56] R.N. Nickolov, R.M. Edreva-Kardjieva, V.J. Kafedjiysky, D.A. Kikolova, N.B. Stankova, D.R. Mehandjiev, Appl. Catal. A 190 (2000) 191.

[57] P. Hou, D. Meeker, H. Wise, J. Catal. 80 (1983) 280.

[58] M. Kantschewa, F. Delannay, H. Jeziorowski, E. Delgado, S. Eder, G. Ertl, J. Catal. 87 (1984) 482.

[59] V. Kettmann, P. Balgavy, L. Sokol, J. Catal. 112 (1988) 93.

[60] M. Łaniecki, M. Małecka-Grycz, F. Domka, Appl. Cata. A 196 (2000) 293.

[61] X.-R. Shi, S.-G. Wang, J. Hu, Y.-Y Chen, Z. Qin, J. Wang, Appl. Cata. A 365 (2009) 62.

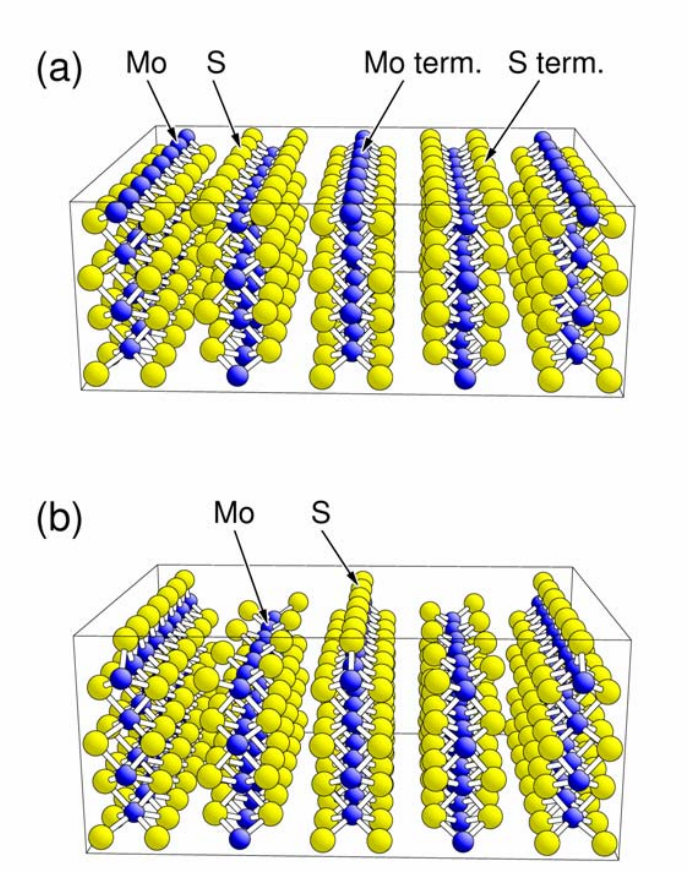
(a)
Mo
S
Mo term.
S term.
(b)
Mo
S

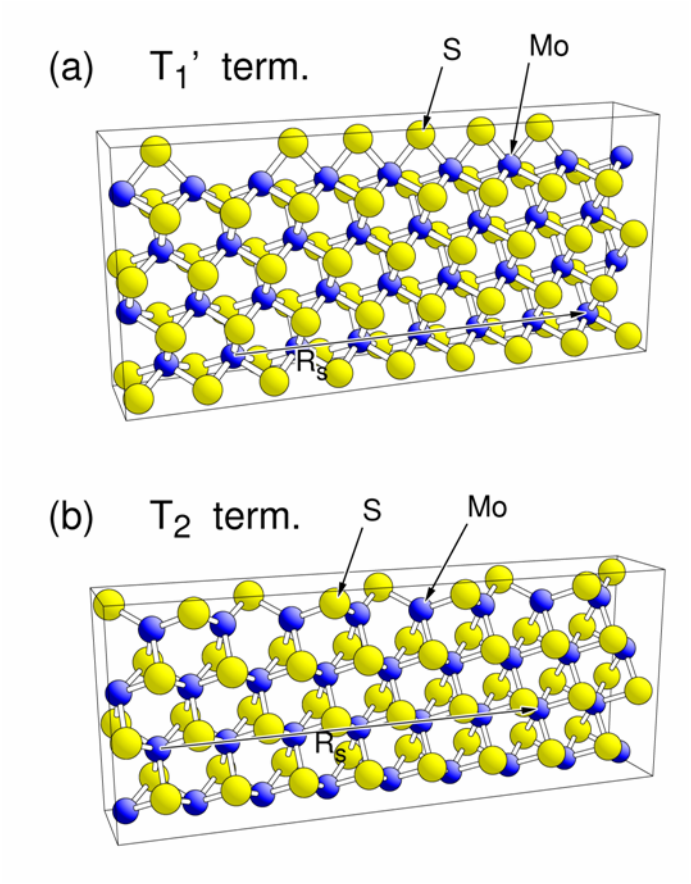
(a) T1' term.
S
Mo
Rs
(b) T2 term.
S
Mo
Rs

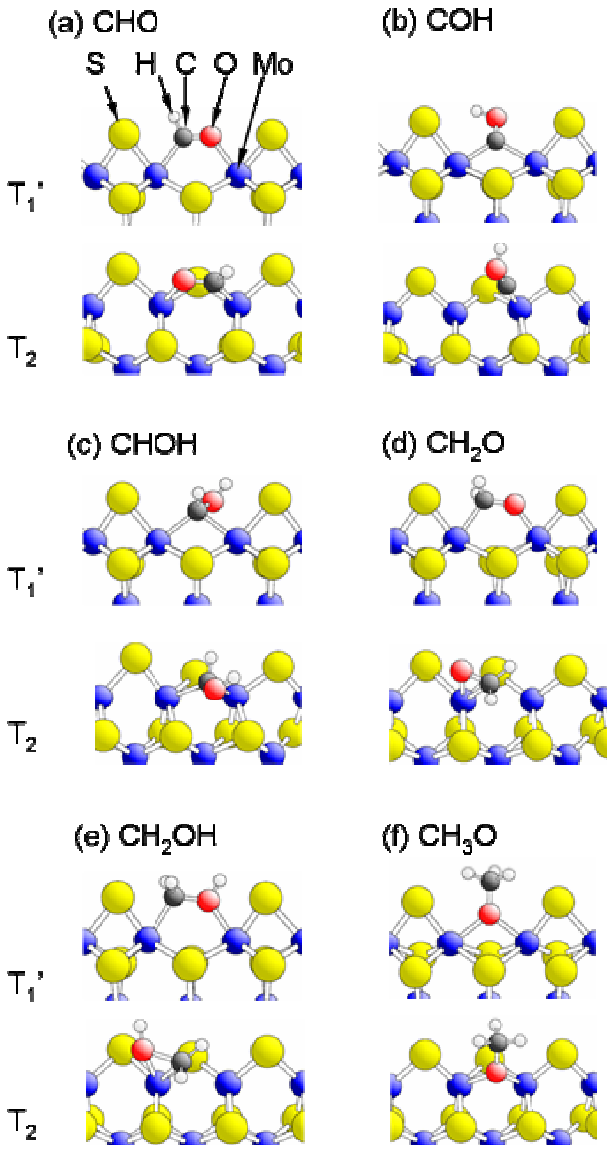
(a) CHO
S H C O Mo
(b) COH
T1'
T2
(c) CHOH
(d) CH2O
T1'
T2
(e) CH2OH
(f) CH3O
T1'
T2

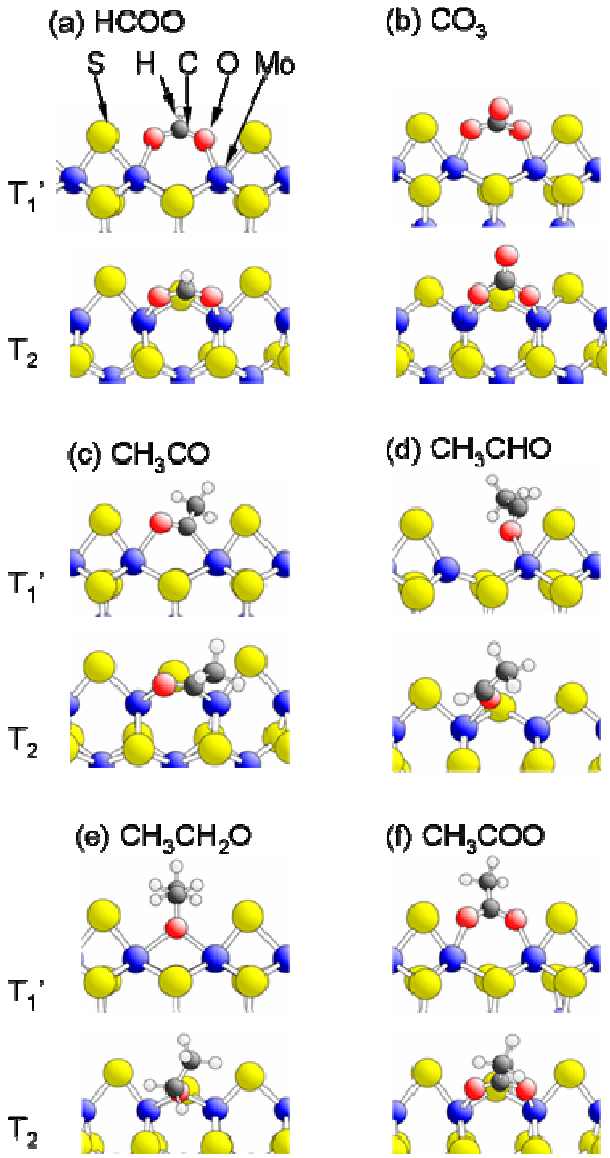
(a) HCOO
S H C O Mo
(b) CO_3
T_1'
T_2
(c) CH_3CO
(d) CH_3CHO
T_1'
T_2
(e) CH_3CH_2O
(f) CH_3COO
T_1'
T_2

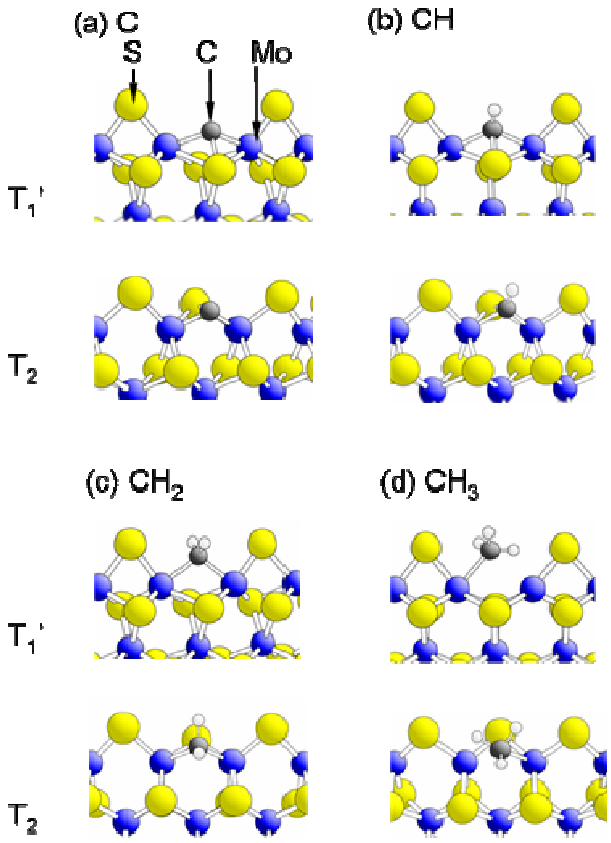
(a) C
S
C
Mo
(b) CH
T1'
T2
(c) CH2
(d) CH3
T1'
T2

(a) $CO + H \longrightarrow CHO$

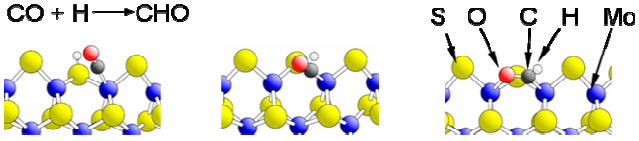

(b) $CHO + H \longrightarrow CH_2O$

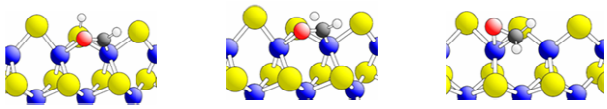

(c) $CH_2O + H \longrightarrow CH_2OH$

$CH_2OH \longrightarrow CH_2 + OH$

(d) $CH_2 + H \longrightarrow CH_3$

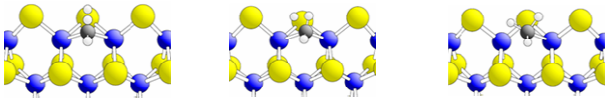

$CH_3 + H \longrightarrow CH_4$

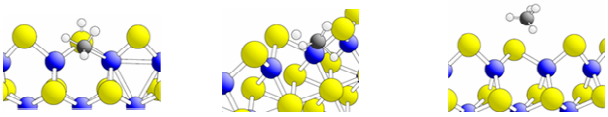

(a) $CO + H \longrightarrow CHO$

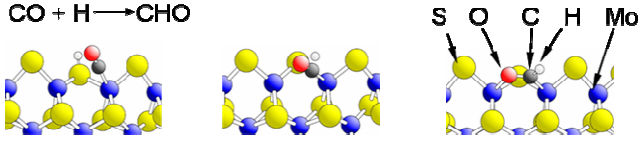

(b) $CHO + H \longrightarrow CH_2O$

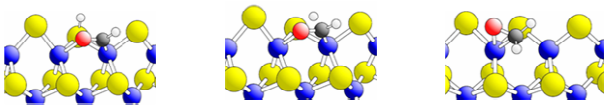

(c) $CH_2O + H \longrightarrow CH_2OH$

$CH_2OH \longrightarrow CH_2 + OH$

(d) $CH_2 + H \longrightarrow CH_3$

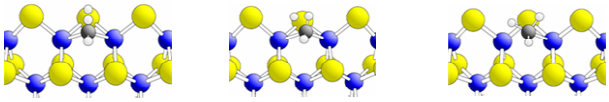

$CH_3 + H \longrightarrow CH_4$

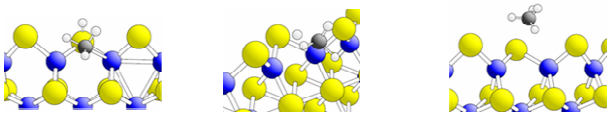

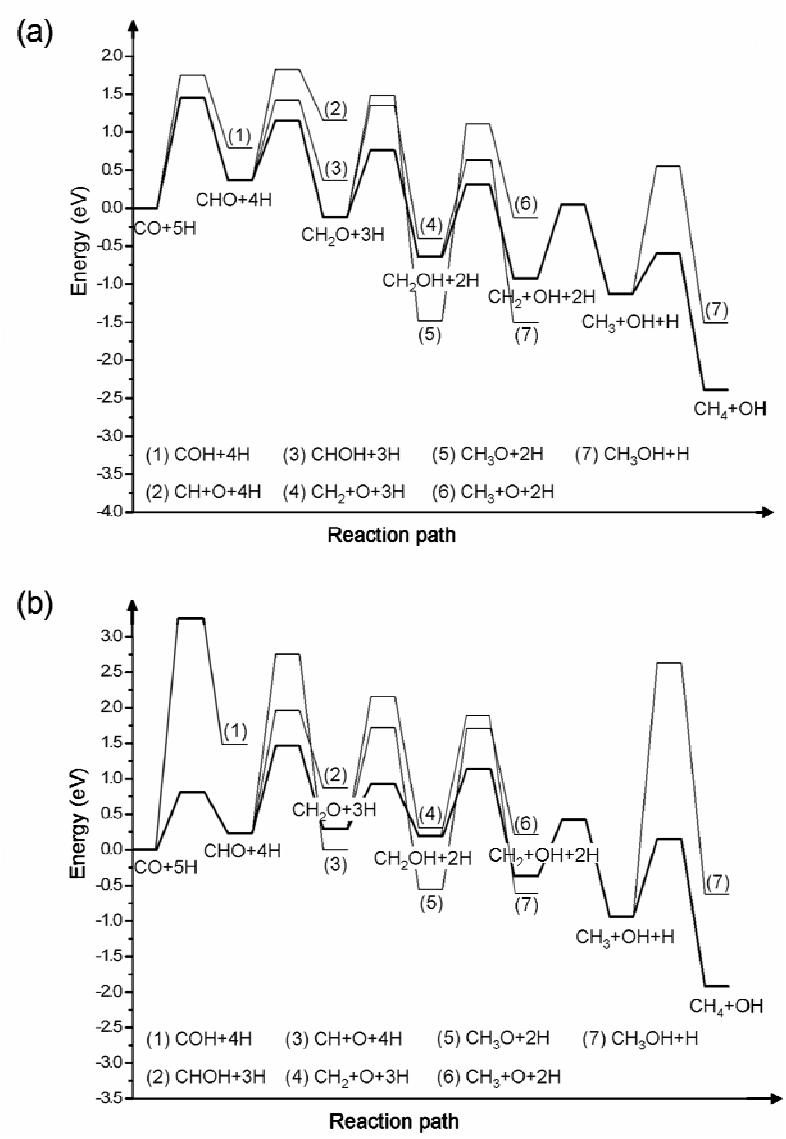
(a)
Energy (eV)
CO+5H
CHO+4H
CH2O+3H
CH2OH+2H
CH2+OH+2H
CH3+OH+H
CH4+OH
(1)
(2)
(3)
(4)
(5)
(6)
(7)
(1) COH+4H (3) CHOH+3H (5) CH3O+2H (7) CH3OH+H
(2) CH+O+4H (4) CH2+O+3H (6) CH3+O+2H
Reaction path
(b)
Energy (eV)
CO+5H
CHO+4H
CH2O+3H
CH2OH+2H
CH2+OH+2H
CH3+OH+H
CH4+OH
(1)
(2)
(3)
(4)
(5)
(6)
(7)
(1) COH+4H (3) CH+O+4H (5) CH3O+2H (7) CH3OH+H
(2) CHOH+3H (4) CH2+O+3H (6) CH3+O+2H
Reaction path